Investigation of in-situ synthesis of alumina reinforcement and comparative flexural behavior with respect to ex-situ Al$_2$O$_3$ reinforced copper composite

Masoud Khodabakhshzade Fallah, Saeid Ghesmati Tabrizi*, Sheida Seyedi

Department of Metallurgy & Ceramics, College of Engineering, Mashhad Branch, Islamic Azad University, Mashhad, Iran.

ABSTRACT

Ex-situ and in-situ reinforced copper matrix composite samples containing 1.1 wt. % and 2 wt. % Al$_2$O$_3$ were produced by spark plasma sintering (SPS) at 830 700 °C with and holding time of 30 20 min. In-situ reinforced sample was synthesized by a novel technique using the reaction between ball-milled copper oxide and Cu-10 wt. % Al filings as the additive materials to and copper powder. The in-situ formation of alumina reinforcement was confirmed by SEM observation and EDS analysis. Morphology and distribution of reinforcement phase in different composite samples were studied. The flexural fracture strength (349 MPa) and strain (0.027) of in-situ reinforced composite were significantly enhanced in addition that it entered the plastic zone. The in-situ reinforced composite sample showed superior flexural fracture strength and strain (349 MPa and 0.027, respectively). The fracture surfaces investigation revealed the effect of clean in-situ interfaces. Different patterns of crack propagation were observed in the SEM images of fracture surfaces: the reinforcement's interface path (due to the formation of undesired oxide phase) was dominant in the ex-situ samples, while the interface of in-situ reinforcements remained intact and the cracks originated in the agglomeration sites.

Keywords: in-situ Al$_2$O$_3$ reinforcement, copper matrix composite, flexural strength, fracture behavior.

1. Introduction

Copper and its alloys take advantage of high thermal and electrical conductivity in such applications as electrical connectors, sliding contacts in electrical machines and railway overhead current collection system, spot and seam resistance welding electrodes, frictional brake parts and integrated circuit sealing materials, where good wear resistance and high thermal and electrical conductivity are needed [1, 2].

However, they may face loss of strength at elevated temperatures due to precipitate coarsening. In order to overcome this issue, vast researches have been conducted to produce copper composites with high electrical and thermal conductivity that retains strength, hardness or wear behavior at elevated temperatures as well. In contrast, ceramic particles dispersion-strengthened copper is able to preserve its strength at elevated temperatures [3, 4].

Oxide dispersion strengthened (ODS) copper matrix composites not only possess good electrical and thermal conductivity but also have higher yield strength and wear resistance. The oxides

usually never dissolve even by heating to the temperatures near the melting point of the metal matrix and dispersion strengthening of composites can be preserved [5].

Different reinforcement phases were incorporated in copper matrix composites, which SiC [6] and MoS_2 [7] particles, hybrid TiB-TiB_2 [8], carbon nanotube [9], and Al_2O_3 particles [10] can be mentioned. Several production routes, for instance, internal oxidation [11], mechanical alloying [12], combustion synthesis [13], friction stir processing [14, 15], powder compaction and sintering [16], ARB [17] and spark plasma sintering (SPS) [18, 19] have been utilized.

In the ex-situ reinforced copper based composites, the scale of alumina reinforcing phase is controlled by the initial powder size and the wettability of the reinforcements by the matrix. This has led to the development of in-situ MMCs, in which the reinforcements are synthesized during the composite processing. [20]. The latter leads to proper particle-matrix interface bonding, enhanced distribution of Al_2O_3 reinforcement, and prevents the coarsening of Al_2O_3 particles and Copper matrix grains [21].

In order to study the mechanical properties, Michalski et al. produced copper nano-composites containing 10 and 20 vol. % Al_2O_3 by SPS and observed the hardness increase with the alumina reinforcing phase content [22].

Also, influence of dispersed Al_2O_3 particles on recrystallization of the matrix grains was studied by Besterci and Kovac [23]. It was observed that fine alumina reinforcing particles obtained by internal oxidation in copper matrix enhanced the wear behavior compared to the competitive Cu-Al alloy [12].

The hardness and thermal stability of Cu-Al_2O_3 composites are dependent on the size and distribution of reinforcement particles in the matrix [24, 25].

In the current study, Al_2O_3 reinforcing particles were incorporated in the copper matrix by two different methods, i.e. ex-situ incorporation and in-situ synthesis . The in-situ reinforcements were produced by low price raw materials of Cu-10 wt. % Al chips . The flexural stress-strain curve of the samples up to fracture was plotted and fractography observation was accomplished to study the load-sharing efficiency of the reinforcing particles in different types of Cu- Al_2O_3 composite samples. The strength of different composite samples and the crack propagation behavior were evaluated.

2. Materials and experimental method

In the present study, copper matrix composite samples, were produced by spark plasma sintering (SPS). Sintering was performed in vacuum. Optical pyrometer, focused on the surface of the die, was used for temperature measurement. Heating rates of 100 °C min^{-1} and 80 °C min^{-1} were used from room temperature to 600 °C and from 600 °C to 830 °C, respectively. The electric current pulsed with 240-40 on-off cycle time.

The ex-situ reinforced samples were prepared by adding Al_2O_3 powder to copper powder. The powders were then mixed in a jar mill for 1 hour. The mixture was consolidated by SPS in a graphite die of diameter and height equal to 50 mm and 10 mm, respectively. The electric current passes through the powder mixture and also graphite die and punch and heats the sample. The maximum temperature and the holding time at the sintering temperature were 830 °C and 30 minutes.

The in-situ reinforced copper sample was prepared with high energy planetary ball milling of the Cu-10 wt. % Al filings, copper oxide and copper powder for 8 hours. The mixture was then sintered by the same SPS procedure.

Equation 1 represents the expected in-situ reaction between additive copper oxide powder and aluminum (available in Cu-10 wt. % Al filings).

$$3CuO + 2Al \rightarrow 3Cu + Al_2O_3 \qquad (1)$$
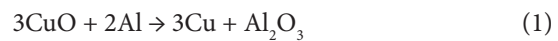
The composite samples compositions (and their respective codes) are listed in table 1.

The metallography samples were prepared by grinding (800 to 2000 meshes) and then polishing by diamond paste. Microstructural studies were carried out by MIRA3 Tescan scanning electron microscope (FE-SEM).

In order to investigate the mechanical behavior of copper matrix composite samples, flexural testing was conducted according to ASTM E290. The flexural test provides tension and compression loading conditions in different sections of the

Table 1- The composite samples composition, processing technique and their respective codes

Type of composite	Al_2O_3 content (wt. %)	Sample name
ex-situ	1.1	SPS 1
	2	SPS 2
in-situ	2	SPS 3

sample. Equations (2, 3) were used to calculate the maximum flexural stress and strain values [26].

$$\sigma = \frac{3PL}{2bd^2} \tag{2}$$

$$\varepsilon = \frac{6\delta d}{L^2} \tag{3}$$

Where, measured values of the applied force (P) and deflection of the midpoint of the sample (δ) are used. Geometrical parameters of the sample are considered as the supports span (L), the width and depth of the sample (b and d respectively).

In addition, the fracture cross sections of the samples were observed by SEM microscope.

3. Results and discussion

The SEM micrographs of the initial materials shows that copper powder used for all composite samples has spherical particles (Fig. 1(a)) and ex-situ Al_2O_3 has the typical morphology of ceramic powder materials (Fig.1 (b)). The SEM images of ball-milled CuO powder plus Bronze filings mixture (that is later used as additive material to copper powder to produce in-situ reinforced composites) are also demonstrated (Fig.1 (c), (d)).

The dispersion of the ex-situ Al_2O_3 reinforcements within the matrix of the sample SPS1 is presented in Fig. 2(a), (b). Elemental EDS analysis result of point A compared to point B (matrix) indicates the presence of Al_2O_3 phase (Fig. 2 (c), (d)). Clustered sites of Al_2O_3 reinforcements in addition to single alumina particles can be observed (Fig.2 (a)). Homogenous distribution of reinforcement phase in the matrix is a challenge in production of MMCs which greatly affects the mechanical properties. Agglomerated reinforcements decrease the strength due to stress concentration.

More precise observation of the SEM microstructure images reveals a third gray phase (point C, Fig. 2(b)) whose EDS analysis (Fig. 2(e)) corresponds to copper oxide phase. This could have been produced as by-product of unintended reaction of alumina and copper during SPS process.

Based on the SEM microstructure images of the sample SPS2, Al_2O_3 reinforcing particles mostly distributed in the grain boundaries (G.B.). Milling of the powder mixture (accomplished in order to reduce the agglomeration of Al_2O_3 reinforcements) has led to some microstructural characteristics after sintering. First, the reinforcing phase are uniformly
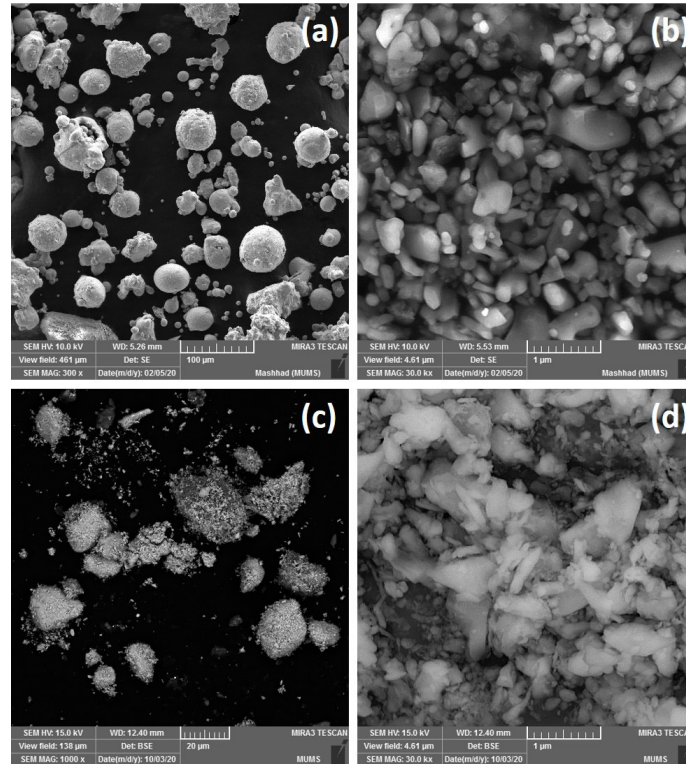

Fig. 1- SEM micrograph of additive materials (a) Copper powder, (b) Alumina powder, (c), (d) the mixture of CuO powder plus bronze filings after 8 h ball-milling, utilized for in-situ synthesis of alumina reinforcements.
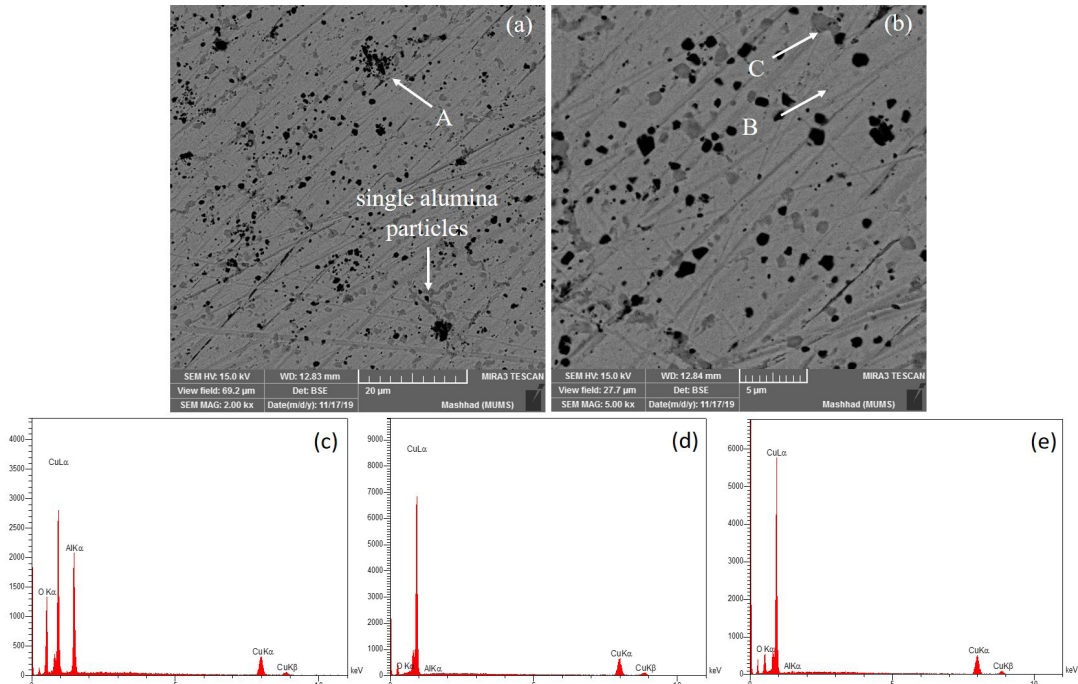
Fig. 2- (a), (b) SEM microstructure images of sample SPS1. Arrow A refers to agglomerated reinforcement particles, arrows B and C refer to the matrix and by-product copper oxide particles, respectively; (c), (d), (e) EDS analysis results of points A, B and C, respectively.
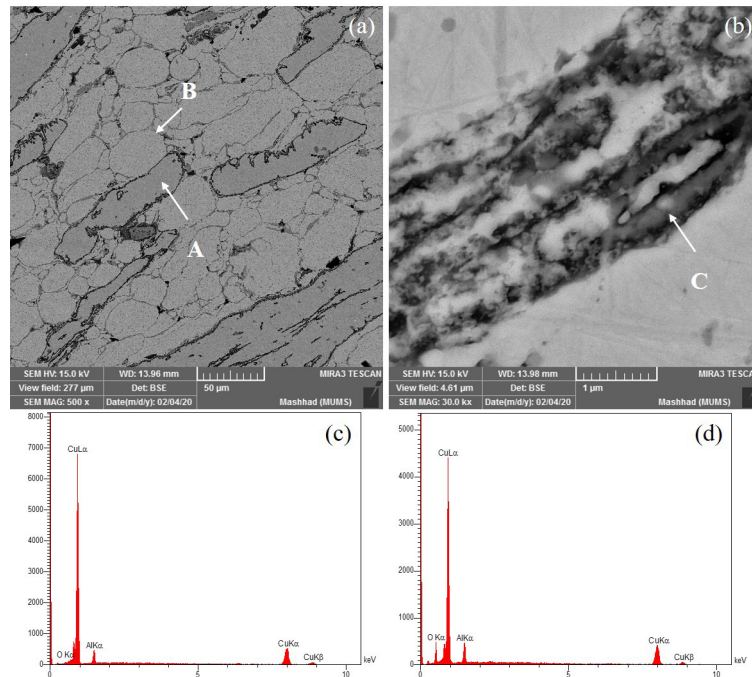

Fig. 3- SEM microstructure images of ex-situ reinforced sample SPS2 illustrating (a) different grain morphologies; A, B pointing to elongated and equiaxed grains, respectively. (b) distribution of alumina reinforcement in the darker G.B. area. EDS analyses presented corresponding to (c) point A (copper grain) and (d) point C (G.B.s containing mixed alumina and copper oxide).

distributed after sintering and agglomeration of Al_2O_3 phase is not observed. Second, different grain morphologies could be observed; elongated grains (Fig. 3(a), arrow A) which were affected by the strain during high energy milling and equiaxed grains (Fig. 3(a), arrow B) formed by the recrystallization process during sintering.

Copper oxide's molecular weight is higher than

alumina, so copper oxide will appear brighter than Al_2O_3 in BSE SEM images. It explains why some G.B. areas are gray and others are black (Fig. 3(a)). It is also notable that darker G.B.'s belong to the elongated grains and recrystallized grains G.B. appear gray, which certifies that Al_2O_3 reinforcements act as barrier in the recrystallization process.

The distribution of Al_2O_3 phase in the darker G.B. area is shown in Fig. 3(b). Comparison of the EDS analysis of points A and C (Fig. 3) verifies the presence of Al_2O_3 reinforcement phase in the darker G.B. locations. It should also be mentioned that the intensity of the copper peak, in the EDS result of gray G.B. areas (point B) is considerable and it hints that copper oxide is produced in high-temperature reactions. This phenomenon is later discussed in the fractography of composite samples.

The feasibility of the synthesis of in-situ Al_2O_3 reinforcing phase was investigated by SEM microstructure observation of the composite sample SPS3 (Fig. 4). Secondary phases are often present in the triangular junction sites of G.B.s (arrows in Fig. 4(a)). Besides, copper matrix grains are mostly equiaxed. Arrow A (Fig. 4(b)) points to a secondary phase particle within the copper matrix; whose elemental EDS analysis verifies the

formation of in-situ Al_2O_3 reinforcement phase in the copper matrix (Fig. 4(c)). The EDS result confirms that the Aluminum atomic percentage matches the value of Al_2O_3 (40 at. %). The in-situ formation of Al_2O_3 reinforcement phase (due to the reaction between additive powders) is driven by stored mechanical energy during milling, as well as the electrical and thermal energy induced during sintering.

Further SEM microstructure observations also confirm the presence of considerable number of single Al_2O_3 reinforcements which are equally spaced in the matrix (Fig. 5(a)). It is expected to enhance the strength of the composite sample.

In-situ Al_2O_3 clustering instances—are also observed (Fig. 5(a), (b)). The angular morphology of the reinforcing particles in the sample SPS3 (with the length of about 3 μm) is consistent with in-situ formed alumina particles by other researchers (e.g. by the method of in-situ reaction synthesis and internal oxidation [27]). The EDS elemental analysis of secondary phase (such as A in Fig. 5(a)) also confirms the in-situ synthesis of alumina phase (Fig. 5(c), (d)). These ceramic reinforcements are formed by the in-situ reaction between the atomic constituents of the ball-milled mixture (i.e. Al from Cu-10% Al filings and oxygen
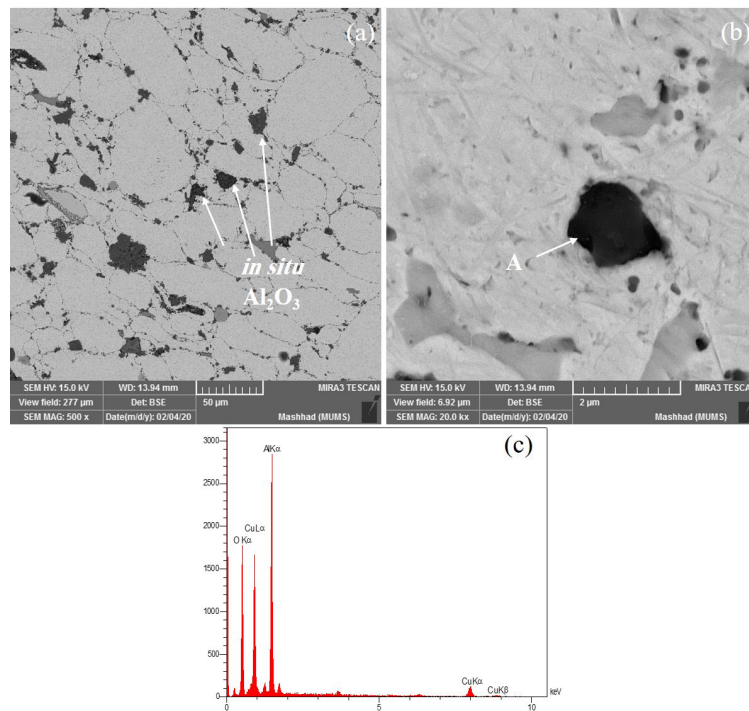

Fig. 4- (a) SEM microstructure image of sample SPS3; Arrows indicate secondary phase particles at the grain boundaries; (b) A secondary phase particle generated after SPS; (c) EDS analysis from point A indicates the formation of in-situ alumina reinforcement.
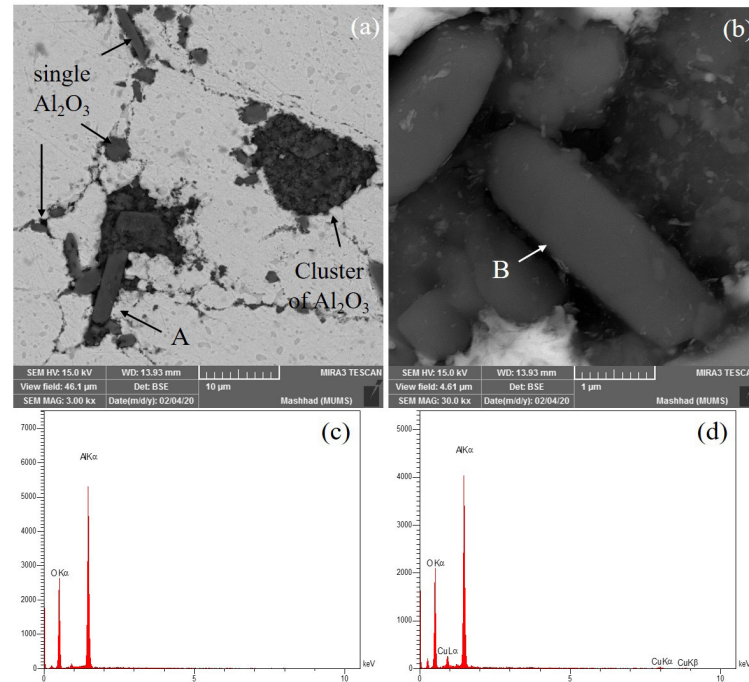
Fig. 5- (a), (b) SEM microstructure images of sample SPS3. Arrow (A) refers to in-situ formed alumina reinforcing particles, (B) refers to an in-situ alumina particle with the length of about 3 μm, (c) EDS elemental analysis of the particle shown with arrow A, (d) EDS elemental analysis of the particle shown with arrow B.

from the copper oxide powder) during SPS.

In order to precisely characterize the Al_2O_3 reinforcement presence and distribution in the composite samples, SEM elemental mapping was carried out (Fig. 6). The distribution of the copper, aluminum and oxygen elements certifies that the second black phases in the G.B. areas are alumina reinforcement clusters. The uniform distribution of Al_2O_3 reinforcements in the G.B. areas of sample SPS2 is asserted, in which their density is higher around the un-recrystallized grains (Fig. 6 (b1-b4)). The in-situ synthesis of Al_2O_3 reinforcement in the sample SPS3 is also approved; the dark phases contain aluminum and oxygen while they lack copper (Fig. 6 (c1-c4)).

Fig. 7 reports the flexural stress-strain behavior of the composite samples. The flexural behavior of composite sample SPS1 is linear to the maximum fracture stress of 338 MPa and strain of 0.014 without any sign of plastic strain. The sample SPS2 showed similar flexural behavior up to the fracture strength of 267 MPa (lower than SPS1) and the fracture strain remained nearly the same as sample SPS1 (both are ex-situ reinforced composite samples). The flexural fracture stress and strain data of the composite samples are summarized in Table 2.

Table 2- Flexural fracture stress and strain values of composite specimens.

Sample name	Fracture Strength (MPa)	Fracture strain
SPS 1	338	0.014
SPS 2	267	0.013
SPS 3	349	0.027

The composite sample SPS3 which contained 2 wt. % in-situ Al_2O_3 reinforcing particles obtained flexural fracture strength equal to 349 MPa (which shows 11 MPa and 82 MPa increase compared to the fracture strengths of ex-situ reinforced composite samples SPS1 and SPS2 , respectively). Furthermore, in-situ alumina reinforcement of copper has led to the increase of the flexural strain twice as much as the ex-situ reinforced composite samples (SPS1 & SPS2).

Besides, the flexural stress-strain curve of sample SPS3 consists of two regions of elastic and plastic behavior (Fig. 7) whose yield stress is determined as 204 MPa by 0.2 % offset method. The elastic part of the in-situ sample SPS3 has also greater slope (i.e. higher value of modulus of elasticity) which confirms the efficiency of in-situ reinforcement.

The sample SPS2 obtained the lowest amount of fracture strength . To summarize , in-situ alumina reinforced composite sample reached higher value
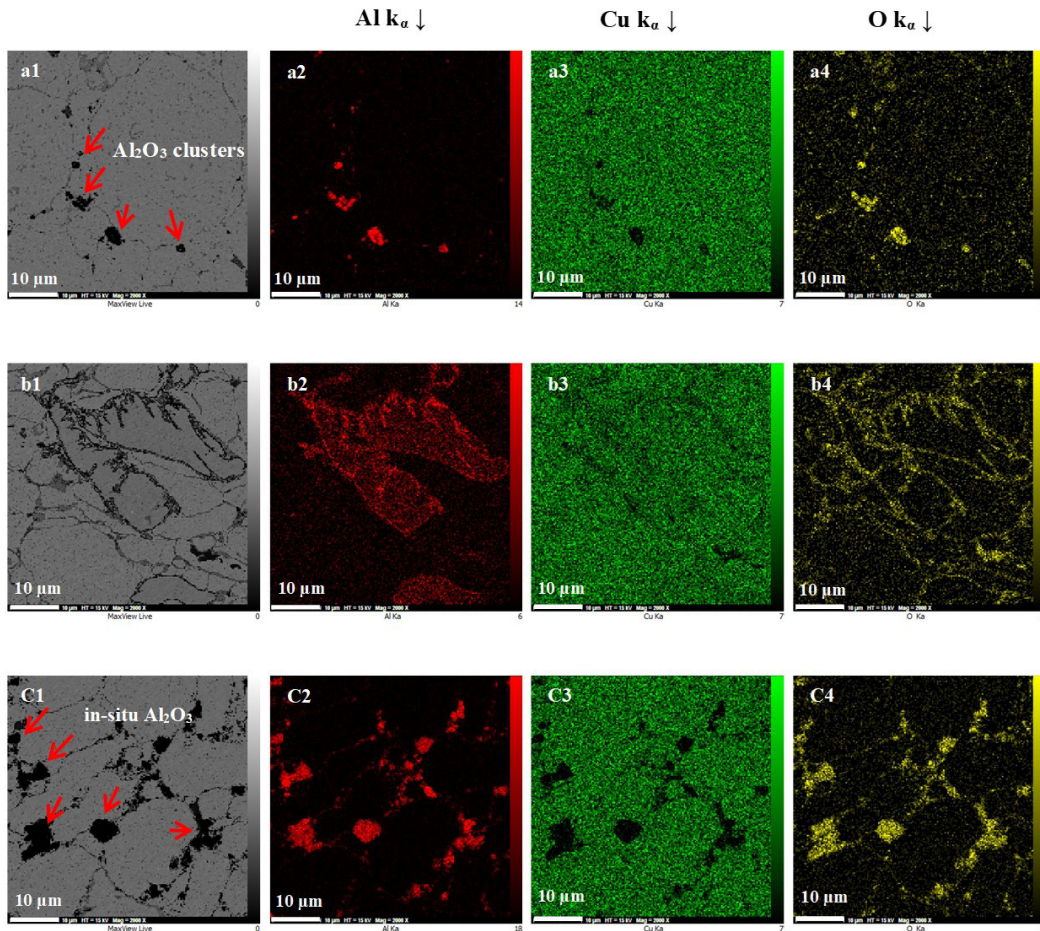
Al k$_a$ ↓   Cu k$_a$ ↓   O k$_a$ ↓

Fig. 6- The SEM microstructure and the distribution mapping of Aluminum, Copper and Oxygen of the sample SPS1 (a1-a4), SPS2 (b1-b4) and SPS3 (C1-C4).
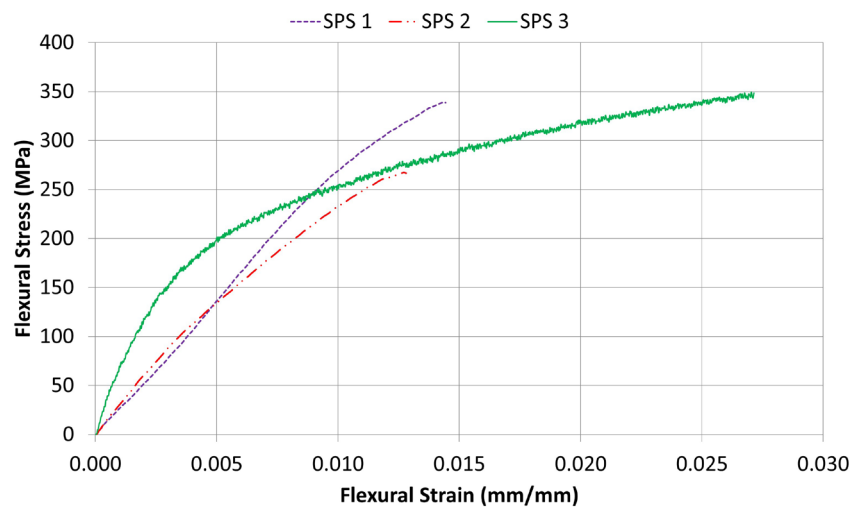
Fig. 7- Flexural stress-strain curves of composite samples.

of flexural fracture strength and strain and also represented plastic yielding .

The fracture surfaces were investigated to evaluate the difference of the flexural behavior of composite samples. The SEM fracture micrographs of the sample SPS1 (Fig. 8) reveal typical cleavage regions and only a small fraction of the surface area is occupied with dimples, which shows that the fracture dominantly had a brittle nature. This is in harmony with the aforementioned fact that

the stress-strain curves of the ex-situ reinforced composite samples presented brittle fracture characteristics. Also it can be observed that micro cracks have propagated on the surface of the sample (Fig. 8 (a), (b)).

An instance of agglomeration of reinforcing particles is shown in the fracture micrograph of sample SPS2 (Fig. 9 (a), (b)) . The EDS analysis indicates the presence of a cluster of alumina particles (Fig. 9 (c)). This may have happened
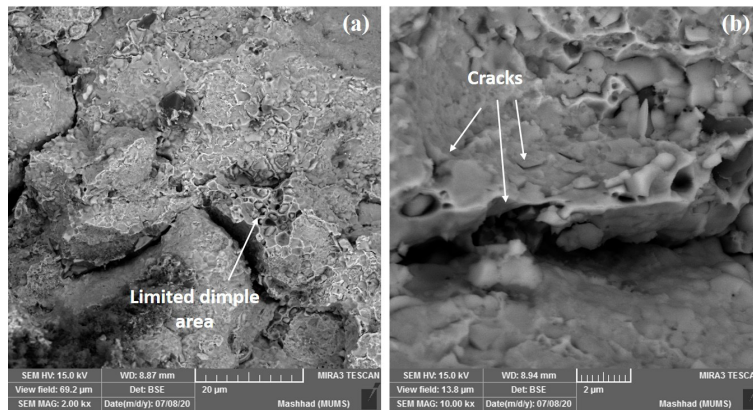

Fig. 8- (a), (b) SEM images of the fracture surface of sample SPS1; cleavage pattern is dominant and a small fraction contributes to dimples.
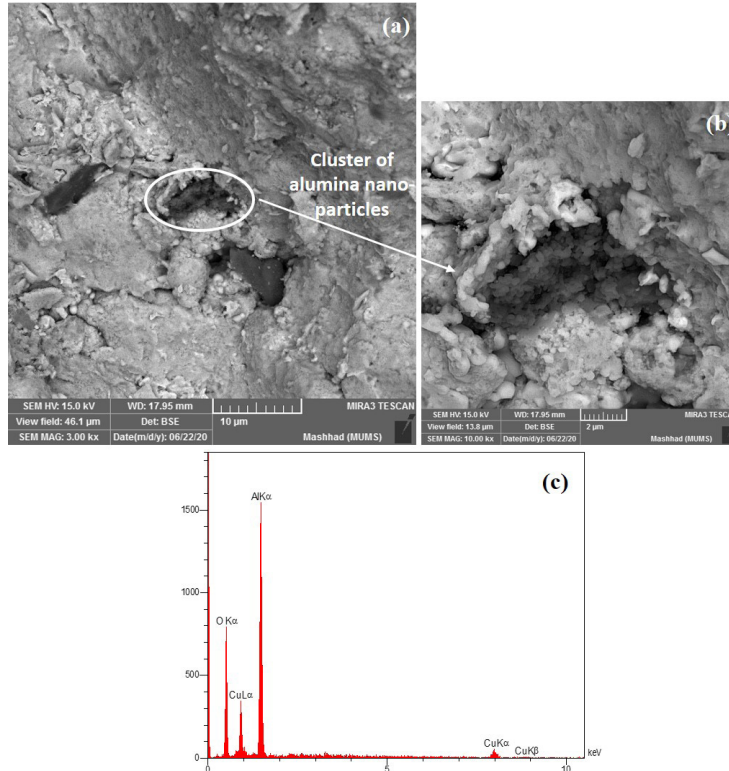

Fig. 9- SEM images of the fracture surface of sample SPS2. (a) alumina reinforcement phase distribution (b) the focused image that indicates clustering of nano-sized alumina particles (c) EDS analysis of cluster area.

during mixing, due to the small particle size of Al_2O_3 powder. The clusters act as stress concentration sites and reduced fracture strength , although the reverse result was expected because of higher reinforcing content of sample SPS2. It seems that hundreds of nano-sized Al_2O_3 particles gathered in a cluster (Fig. 9 (b)). Cleavage pattern of the fracture surface is also observed (Fig. 9 (a)).

Further investigation of the fracture surface SEM images of sample SPS2 (Fig. 10(a), (b)) shows that a propagating crack passed adjacent to particle A, whose morphology and EDS analysis (Fig. 10(c)) prove it to be an Al_2O_3 particle. The crack almost de-bonded the matrix-reinforcement interface.

Light colored particles, which are attached to Al_2O_3 reinforcements interface, whose EDS elemental analysis (Fig. 10(e)) reveals they are The copper oxide that is a brittle by-product of the sintering process disrupts the load sharing between the matrix and reinforcement phase. It can explain the loss of strength of the sample SPS2 compared to SPS1 in spite of higher reinforcement content.

Fig. 11 shows the fracture cross section of the sample SPS3 whose microstructure analysis results were in favor of in-situ Al_2O_3 phase formation. Compared to the ex-situ samples, distinctive

features have appeared . First, dimples with the approximate diameter of 5-10 μm are visible all over the fracture surfaces (Fig. 11(a)), which contribute to the plastic deformation of the sample during flexural loading. The dimples are more numerous and have larger size compared to the composite samples SPS1 and SPS2.

The second feature is that the cracks are nucleated in the Al_2O_3 reinforcement phase and then penetrated into the matrix (Fig. 11(b)), where the ductile matrix is able to absorb the energy and the crack length is limited in the matrix (crack-tip plastic blunting by a ductile metallic phase). This proves that there's good load-sharing efficiency from the matrix to the in-situ reinforcement phase so that the great extent of the applied stress is tolerated by the reinforcement phases. Meanwhile, strong matrix-reinforcement bond (mainly due to the absence of oxide by-products confirmed by EDS analysis in Fig. 11(c), (d)) delayed or prevented the interface crack formation, hence the load capability of the system increased. That's why the matrix exhibited more significant evidence of the plastic deformation compared to the ex-situ reinforced samples. It is in harmony with the flexural stress-strain behavior of sample SPS3.
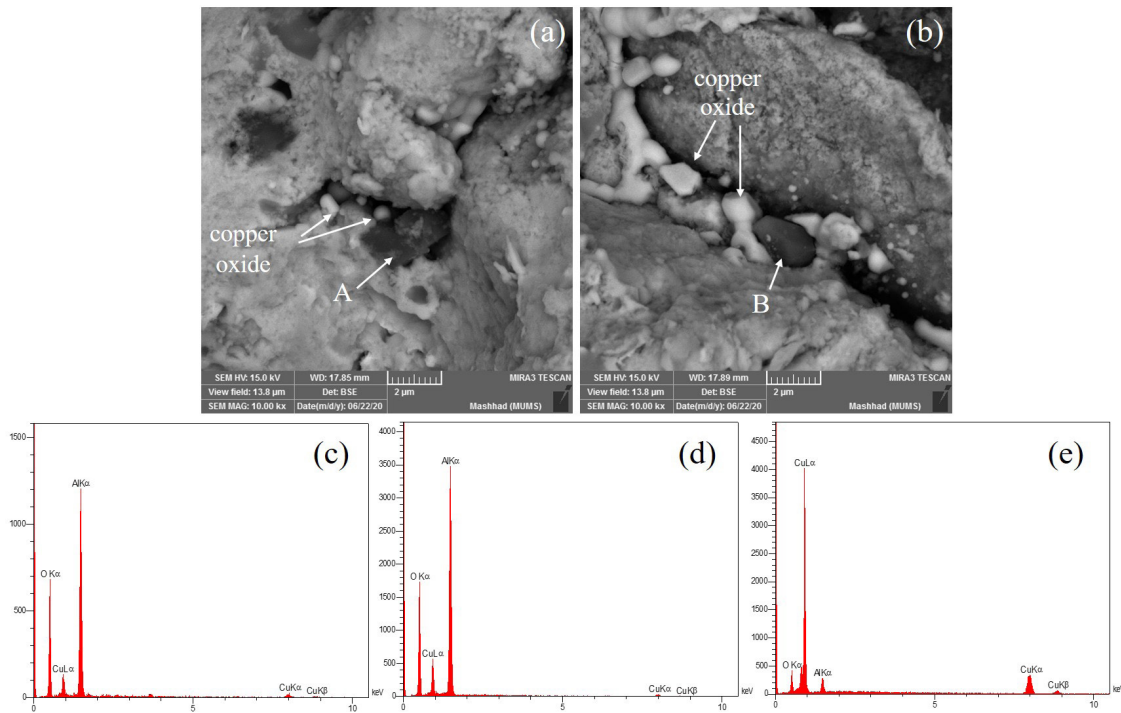

Fig. 10- (a) , (b) SEM micrographs of fracture cross section of sample SPS2, (c) , (d) EDS analysis of points A, B which confirm they are Al_2O_3 reinforcements, (e) EDS analysis of light colored interfacial phases that shows they are made up of copper oxide.
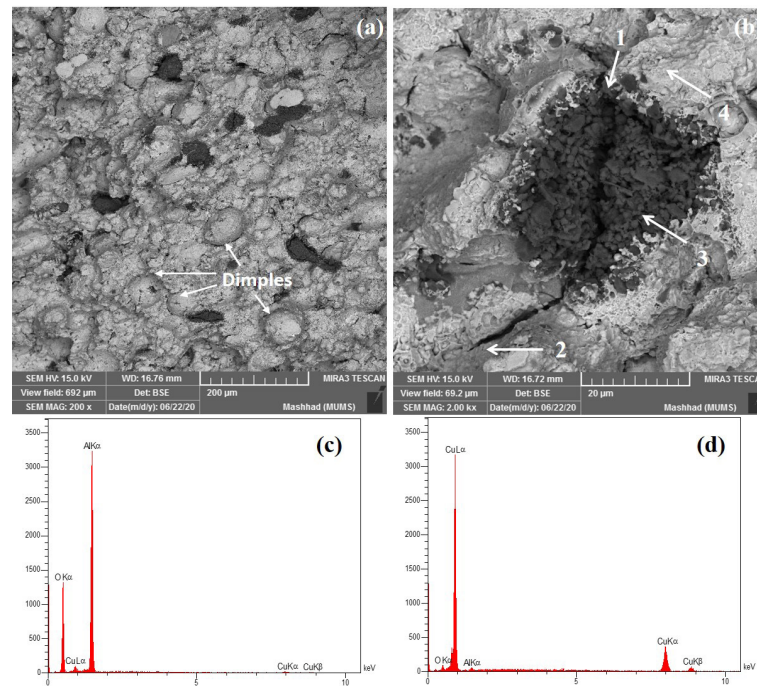
Fig. 11- (a) SEM images of fracture surface of sample SPS3; the general distribution of the reinforcement phase within the matrix, (b) the appearance of an in-situ Al_2O_3 reinforcement phase which is cracked; arrow 1 indicates the nucleation site of the crack, while arrow 2 refers to the crack tip plastic blunting in the metal matrix. (c) EDS analysis of point 3 indicates the presence of alumina phase without contamination; (d) EDS analysis of the matrix (arrow 4 in (b)) as reference.

4. Conclusion

1. Ex-situ Al_2O_3 reinforced copper composite samples contained both single distribution and agglomeration of reinforcing particles.

2. SPS processing of the mixture of copper powder and the ball milled additive containing copper oxide plus Cu-10%Al filings has successfully led to the synthesis of in-situ Al_2O_3 reinforcing phase.

3. Flexural stress-strain behavior of the ex-situ 1.1 & 2 wt. % Al_2O_3 reinforced composites exhibit elastic behavior with the respective flexural strength values of 338 MPa and 267 MPa, while both samples' flexural strain reached the same value of 0.014.

4. Flexural fracture strength of the in-situ 2 wt. % Al_2O_3 reinforced sample increased considerably compared to other samples. The ultimate flexural strain of the in-situ 2 wt. % Al_2O_3 sample also increased approximately twice value . Furthermore, the increase of the elastic modulus confirms better efficiency of in-situ reinforcement.

5. The fracture cross-section of the ex-situ reinforced samples exhibited more brittle features. Easier crack propagation path (due to the presence of unintended reaction product phase of copper oxide), in conjunction with agglomeration of reinforcements lowered the strength and the ductility of ex-situ reinforced samples.

6. The SEM fracture micrographs of in-situ 2 wt. % Al_2O_3 reinforced sample, exhibited far more ductile features.

7. Different crack propagation path in the composite samples is the key factor that differentiates the plastic and elastic flexural behavior of composite samples; cracks initiated within the Al_2O_3 reinforcement and then penetrated into the matrix of in-situ reinforced sample, while cracks were mainly propagated in the reinforcements interface of the ex-situ reinforced samples).

References

1. Lee DW, Ha GH, Kim BK. Synthesis of Cu-Al 2 O 3 nano composite powder. Scripta Materialia. 2001;44(8-9):2137-40.
2. Fu Y, Pan Q, Cao Z, Li S, Huo Y. Strength and electrical conductivity behavior of nanoparticles reaction on new alumina dispersion-strengthened copper alloy. Journal of Alloys and Compounds. 2019;798:616-21.
3. Zhang X, Lin C, Cui S, Li Z. Characteristics of Nano-alumina Particles Dispersion Strengthened Copper Fabricated by Reaction Synthesis. Rare Metal Materials and Engineering. 2016;45(4):893-6.

4. Tjong SC, Lau KC. Tribological behaviour of SiC particle-reinforced copper matrix composites. Materials Letters. 2000;43(5-6):274-80.

5. Guobin L, jibing S, Quanmei G, Ru W. Fabrication of the nanometer Al2O3/Cu composite by internal oxidation. Journal of Materials Processing Technology. 2005;170(1-2):336-40.

6. Qin YQ, Wu YC, Wang DB, Li P, Huang XM, Zheng YC. Influence of SiC Particle Size on the Wear Properties of SiC/Cu Composites. Advanced Materials Research. 2011;311-313:635-9.

7. Moazami-Goudarzi M, Nemati A. Tribological behavior of self lubricating Cu/MoS2 composites fabricated by powder metallurgy. Transactions of Nonferrous Metals Society of China. 2018;28(5):946-56.

8. Liang S, Li W, Jiang Y, Cao F, Dong G, Xiao P. Microstructures and properties of hybrid copper matrix composites reinforced by TiB whiskers and TiB2 particles. Journal of Alloys and Compounds. 2019;797:589-94.

9. Shuai J, Xiong L-q, Zhu L, Li W-z. Effects of ply-orientation on microstructure and properties of super-aligned carbon nanotube reinforced copper laminar composites. Transactions of Nonferrous Metals Society of China. 2017;27(8):1747-58.

10. Qin YQ, Tian Y, Peng YQ, Luo LM, Zan X, Xu Q, et al. Research status and development trend of preparation technology of ceramic particle dispersion strengthened copper-matrix composites. Journal of Alloys and Compounds. 2020;848:156475.

11. Soleimanpour AM, Abachi P, Purazrang K. Wear behaviour of in situ Cu–Al2O3 composites produced by internal oxidation of as cast alloys. Tribology - Materials, Surfaces & Interfaces. 2009;3(3):125-31.

12. Ying DY, Zhang DL. Processing of Cu–Al2O3 metal matrix nanocomposite materials by using high energy ball milling. Materials Science and Engineering: A. 2000;286(1):152-6.

13. Xu Q, Zhang X, Han J, He X, Kvanin VL. Combustion synthesis and densification of titanium diboride–copper matrix composite. Materials Letters. 2003;57(28):4439-44.

14. Dinaharan I, Sathiskumar R, Murugan N. Effect of ceramic particulate type on microstructure and properties of copper matrix composites synthesized by friction stir processing. Journal of Materials Research and Technology. 2016;5(4):302-16.

15. Sudhakar M, Srinivasa Rao CH, Saheb KM. Production of Surface Composites by Friction Stir Processing-A Review. Materials Today: Proceedings. 2018;5(1):929-35.

16. Prakash KS, Thankachan T, Radhakrishnan R. Parametric optimization of dry sliding wear loss of copper–MWCNT composites. Transactions of Nonferrous Metals Society of China. 2017;27(3):627-37.

17. Jamaati R, Toroghinejad MR. Application of ARB process for manufacturing high-strength, finely dispersed and highly uniform Cu/Al2O3 composite. Materials Science and Engineering: A. 2010;527(27-28):7430-5.

18. Wang H, Zhang Z-H, Hu Z-Y, Song Q, Yin S-P, Kang Z, et al. Improvement of interfacial interaction and mechanical properties in copper matrix composites reinforced with copper coated carbon nanotubes. Materials Science and Engineering: A. 2018;715:163-73.

19. Pan Y, Xiao S, Lu X, Zhou C, Li Y, Liu Z, et al. Fabrication, mechanical properties and electrical conductivity of Al2O3 reinforced Cu/CNTs composites. Journal of Alloys and Compounds. 2019;782:1015-23.

20. Ritasalo R, Liua XW, Söderberg O, Keski-Honkola A, Pitkänen V, Hannula SP. The Microstructural Effects on the Mechanical and ThermalProperties of Pulsed Electric Current Sintered Cu-Al2O3 Composites. Procedia Engineering. 2011;10:124-9.

21. Zhang X-H, Li X-X, Chen H, Li T-B, Su W, Guo S-D. Investigation on microstructure and properties of Cu–Al2O3 composites fabricated by a novel in-situ reactive synthesis. Materials & Design. 2016;92:58-63.

22. Michalski A, Jaroszewicz J, Rosiński M, Siemiaszko D, Kurzydlowski KJ. Nanocrystalline Cu-Al$_2$O$_3$ Composites Sintered by the Pulse Plasma Technique. Solid State Phenomena. 2006;114:227-32.

23. Besterci M, Kovac L. Microstructure and properties of Cu-Al$_2$O$_3$ composites prepared by powder metallurgy. International Journal of Materials and Product Technology. 2003;18(1/2/3):26.

24. Guo X, Song K, Liang S, Wang X, Zhang Y. Effect of Al2O3 Particle Size on Electrical Wear Performance of Al2O3/Cu Composites. Tribology Transactions. 2016;59(1):170-7.

25. Mamedov V. Spark plasma sintering as advanced PM sintering method. Powder Metallurgy. 2002;45(4):322-8.

26. Dowling NE. Mechanical behavior of materials: engineering methods for deformation, fracture, and fatigue. Prentice-Hall int, Englewood Cliffs, New Jersey, 1993.

27. Zhang X-h, Li X-x. Characteristics of alumina particles in dispersion-strengthened copper alloys. International Journal of Minerals, Metallurgy, and Materials. 2014;21(11):1115-9.